Charge optimized many-body (COMB) potential for dynamical simulation of Ni–Al phases

2015 J. Phys.: Condens. Matter 27 336302

(http://iopscience.iop.org/0953-8984/27/33/336302)

IOP Publishing Journal of Physics: Condensed Matter
J. Phys.: Condens. Matter **27** (2015) 336302 (9pp) doi:10.1088/0953-8984/27/33/336302

Charge optimized many-body (COMB) potential for dynamical simulation of Ni–Al phases

Aakash Kumar, Aleksandr Chernatynskiy, Tao Liang, Kamal Choudhary, Mark J Noordhoek[1], Yu-Ting Cheng[2], Simon R Phillpot and Susan B Sinnott[3]

Department of Materials Science and Engineering, University of Florida, Gainesville, FL 32611–6400, USA

E-mail: ssinn@mse.ufl.edu

Received 20 May 2015, revised 25 June 2015
Accepted for publication 9 July 2015
Published 3 August 2015

Abstract

An interatomic potential for the Ni–Al system is presented within the third-generation charge optimized many-body (COMB3) formalism. The potential has been optimized for Ni_3Al, or the γ' phase in Ni-based superalloys. The formation energies predicted for other Ni–Al phases are in reasonable agreement with first-principles results. The potential further predicts good mechanical properties for Ni_3Al, which includes the values of the complex stacking fault (CSF) and the anti-phase boundary (APB) energies for the (1 1 1) and (1 0 0) planes. It is also used to investigate dislocation propagation across the Ni_3Al (1 1 0)–Ni (1 1 0) interface, and the results are consistent with simulation results reported in the literature. The potential is further used in combination with a recent COMB3 potential for Al_2O_3 to investigate the Ni_3Al (1 1 1)–Al_2O_3 (0 0 0 1) interface, which has not been modeled previously at the classical atomistic level due to the lack of a reactive potential to describe both Ni_3Al and Al_2O_3 as well as interactions between them. The calculated work of adhesion for this interface is predicted to be 1.85 J m^{-2}, which is in agreement with available experimental data. The predicted interlayer distance is further consistent with the available first-principles results for Ni (1 1 1)–Al_2O_3 (0 0 0 1).

Keywords: molecular dynamics (MD), interface, Ni, Ni_3Al, Ni_3Al–Al_2O_3, charge optimized many-body (COMB), interatomic potential

(Some figures may appear in colour only in the online journal)

1. Introduction

Nickel-based superalloys are used in sections of gas turbines, which face extreme temperature conditions [1]. The two phases present in these alloys are the γ phase, which is a Ni matrix, and the γ' phase composed of Ni_3Al, which accounts for around 70 vol. %. The precipitation hardened γ' phase is responsible for the great strength of this material. The superior mechanical performance of the superalloys is due to the yield stress anomaly of the γ' phase wherein its yield strength increases with temperature up to a critical limit. Thus, Ni_3Al has become a particularly important intermetallic compound that has been extensively studied over the years [1, 2]. The other common nickel aluminide, NiAl, is another high temperature material that is brittle at room temperature, which limits its applicability [3].

[1] Present address: Department of Mechanical Engineering, University of South Carolina, Columbia, SC 29208, USA.
[2] Present address: Department of Materials Science and Engineering, Johns Hopkins University, Baltimore, MD 21218–2681, USA.
[3] Author to whom any correspondence should be addressed.

Although first-principles calculations provide an accurate description of a material's properties at 0 K, they are limited to system sizes of a few hundred atoms. While *ab initio* molecular dynamics (MD) [4] simulations provide a first-principles approach to simulating materials at finite temperatures, it is generally computationally intensive and limited to a relatively small number of atoms. Thus, MD simulations [5, 6] based on classical potentials have become the method of choice to investigate the properties of materials that depend on microstructure such as dislocations, grain boundaries, and interfaces at the atomic scale. This is because a sizeable number of atoms are needed for such studies due to the strain fields associated with microstructural features.

To carry out such MD simulations, an interatomic potential is needed that can reproduce the different properties of the system being studied and is able to predict new properties of interest. Two interatomic potentials for the Ni–Ni_3Al system have been especially popular [7, 8] and both are based on the embedded atom method (EAM) formalism. While the Voter–Chen potential [8] is widely used for simulating the dynamical behaviour of Ni and Ni_3Al, it was not intended to describe the other phases of the Ni–Al system. The more recent EAM potential developed by Pun and Mishin [7] accurately reproduces the formation energies of several phases of the Ni–Al. It also does a good job of describing point defects and planar defects within Ni_3Al. However, EAM potentials are best suited for metallic systems. A potential formalism with dynamically varying charge would be required to capture the influence of Al_2O_3 film formation on Ni-based superalloys following the introduction of oxygen at high temperatures [9], or to model thermal barrier coatings on the Ni-based superalloy gas-turbines [10].

Here, we present a new potential under the third-generation charge optimized many-body (COMB3) formalism [11, 12] for simulating the γ and γ' phases of nickel superalloys. In particular, we present an interatomic potential for the pure Ni and the Ni–Al system that makes use of a previously published COMB3 potential for Al [13]. Besides the EAM potential by Pun and Mishin [7], no other potential has been disseminated for the Ni–Al system that also includes the B2–NiAl phase. The new COMB3 potential also reproduces the energetics of additional Ni–Al phases. In addition, we present a COMB3 potential for the Ni–Al–O system that is used in combination with a previously published Al_2O_3 COMB3 potential [14] to model the Ni_3Al–Al_2O_3 interface and predict correct adhesion behaviour.

The rest of the paper is organized as follows. The specifies of the COMB3 formalism and the parameterization details are provided in section 2. This is followed by the results and discussion of the properties of Ni and Ni_3Al in section 3. Lastly, we provide conclusions in section 4.

2. Details of the COMB3 potential

2.1. COMB3 Formalism

The COMB3 potential evolved from the second-generation version, known as COMB2 [15], which has its origin in the Tersoff potential [16], with a scheme for dynamic charge equilibration. Equation (1) provides the different components of the COMB3 potential energy function. The total energy of the system is expressed as a sum of its (i) electrostatic energy (U^{es}), (ii) energy due to short-range interactions (U^{short}), (iii) energy due to van der Waals interactions (U^{vdW}), and lastly, (iv) correction terms, $U^{\text{corr}}[\{r\}]$. Here $\{q\}$ and $\{r\}$ refer to the charge and coordinates of the atoms in the system, respectively.

$$U^{\text{tot}}[\{q\},\{r\}] = U^{\text{es}}[\{q\},\{r\}] + U^{\text{short}}[\{q\},\{r\}] + U^{vdW}[\{r\}] + U^{\text{corr}}[\{r\}] \tag{1}$$

More specifically, U^{es} takes into account the energy to ionize an atom, the energy associated with the interaction between two charges, and between the charge and nucleus, and energies related to polarizability. U^{short} is composed of energies due to pairwise attractive and repulsive terms. U^{vdW} is evaluated via a standard Lennard–Jones expression. The U^{corr} correction terms are used to prevent unphysical system behaviour. These correction terms include functions for (i) angular corrections, (ii) bond bending corrections, (iii) additional repulsion corrections, (iv) over-coordination correction, and (v) charge barrier correction. A complete description of all the components of the COMB3 formalism can be found elsewhere [12].

In the present version of COMB3, we have modified the charge barrier function, which is one of the terms within the U^{corr} term in equation (1). This is a correction term for U^{es} to penalize the partial charges on individual atoms outside a defined range. The charge barrier function has been modified from its original form (equation (60) in [12]) to the one shown below in equation (2).

$$V_i^{\text{Barrier}}(q_i) = \begin{cases} \chi_i(q_{\min} - q_i) + J_i(q_{\min} - q_i)^2, & q_i < q_{\min} \\ 0, & q_{\min} < q_i < q_{\max} \\ \chi_i(q_i - q_{\max}) + J_i(q_i - q_{\max})^2, & q_i > q_{\max} \end{cases} \tag{2}$$

Here $q_{\min}$ and $q_{\max}$ are the lower and upper charge limits of an element. In particular, the values are −0.9 and 4.0 for Ni, −0.9 and 3.0 for Al, and −2 and 0.9 for O, respectively. Overall, the charge barrier function is an *ad hoc* function that prevents charges from dynamically varying and attaining unphysical values.

2.2. Parameterization of Ni

The training database for the parameterization of Ni consisted of the ground state, or the face-centered-cubic (FCC) phase; additional non-existent phases to provide energies as a function of differing numbers of neighbors, including hexagonal-close-packed (HCP), body-centered-cubic (BCC), diamond-cubic, simple-cubic (SC); the (1 0 0), (1 1 0) and (1 1 1) surfaces of fcc nickel; the unstable and stable stacking fault structures of

Table 1. Properties of pure Ni computed using EAM and COMB3 potentials compared to the results of experimental measurements and DFT calculations.

	Expt.[a,b,c,f]/DFT[d,e]	EAM[g]	MEAM[h]	EAM[i] Voter–Chen	EAM[j] Pun–Mishin	COMB3 (this work)
a(Å)	3.52[a]	3.52	3.52	3.52	3.52	3.52
E_c (eV/atom)	−4.45[b]	−4.45	−4.45	−4.45	−4.45	−4.45
C_{11} (GPa)	261[c]	263	261	244	241	259
C_{12} (GPa)	151[c]	154	151	149	151	148
C_{44} (GPa)	132[c]	127	132	126	127	113
B (GPa)	188	186	188	181	181	185
G (GPa)	101	84	101	—	94	90
γ (1 0 0) (mJ m^{-2})	2426[d]	2212	1943	—	1933	2370
γ (1 1 0) (mJ m^{-2})	2368[d]	2359	2057	—	2084	2445
γ (111) (mJ m^{-2})	2011[d]	2059	1606	—	1757	1912
$\gamma_{unstable}$ (mJ m^{-2})	233[e]	355	—	230[k]	310	254
γ_{sf} (mJ m^2)	125[e]	103	—	59[k]	135	120
V_{Ni} (eV/atom)	1.6[f]	1.12	1.51	—	1.57	1.64
int_{Ni} (eV/atom)	—	4.48	4.48	—	3.95	4.61

[a] [21],
[b] [22],
[c] [23],
[d] [24],
[e] [25],
[f] [26],
[g] [27],
[h] [28],
[i] [8],
[j] [7],
[k] [29].

fcc Ni; structures of fcc Ni containing, (i) an octahedral self-interstitial of Ni, and (ii) a Ni vacancy. Optimization of the parameters was carried out by minimizing the cost function with weights on different energies of the above structures to fit target energies from experimental and/or first-principles density functional theory (DFT) results. The DFT values listed here use the exchange-correlation functional of Perdew, Burke and Ernzerhof within the generalized gradient approximation (PBE-GGA) [17, 18]. Besides the cohesive, surface and stacking fault energies, the elastic constants of the FCC phase were also included in the fitting. The fitting procedure was carried out using the methodology of potential optimization software for Materials (POSMat) [19] using a Simplex algorithm [20].

The present interatomic potential is able to correctly reproduce the correct formation energies, elastic constants, surface and stacking fault energies for Ni. These results are summarized in table 1.

2.3. Parameterization of the Ni–Al system

The training database for the Ni–Al parameterization consisted of different crystalline phases of Ni_3Al ($L1_2$ structure) and NiAl (B2 structure); the (1 0 0), (1 1 0) and (1 1 1) surfaces of $L1_2$–Ni_3Al; the DO_{22} polymorph of Ni_3Al and rocksalt structured polymorph of NiAl; and $L1_2$–Ni_3Al structures with defects, namely, an Al vacancy, a Ni vacancy, an Al interstitial and, a Ni interstitial. The DO_{22} structure has a heat of formation very close to that of the $L1_2$ phase, making it especially important for inclusion in the fitting database. The properties fit were the heats of reaction and the elastic constants of $L1_2$–Ni_3Al and B2–NiAl as well as the surface energies of $L1_2$–Ni_3Al. The phonon-dispersion energies were not included in the fitting database. The parameterization was carried out using the same procedure discussed in section 2.2.

Tables 2 and 3 provide the results obtained for properties of Ni_3Al and NiAl, respectively, as predicted by COMB3 and other methods. These properties were part of the fitting database used to parameterize COMB3. More weight was given to the properties of Ni_3Al as it is the alloy of most interest for superalloys. It can be seen that the properties of Ni_3Al are in close agreement to those measured in experiments and predicted by DFT calculations. In particular, the predicted values of the lattice constant and cohesive energy are in very good agreement with the experimental results. A comparison is also provided to a high quality EAM potential for Ni–Al by Pun and Mishin [7].

2.4. Parameterization of the Ni–O system

The NiO-rocksalt structure was also parameterized in order to limit the core charges for Ni. In particular, as charges were not involved in the parameterization of pure Ni, we used NiO to constrain the charge on Ni so that the pure Ni is transferrable to NiO and other oxide structures. It should be noted that in this case the fitting database included only the NiO rocksalt phase. The resulting COMB3 potential is in good agreement

Table 2. Properties of Ni_3Al computed using EAM and COMB3 potentials compared to the results of experimental measurements and DFT calculations.

	Expt.[a,b,c] / DFT[d,e]	EAM Pun–Mishin[d]	EAM Voter–Chen[f]	COMB3 (this work)
a(Å)	3.57[a]	3.53	3.57	3.56
E_c (eV/atom)	−4.57[b]	−4.62	−4.59	−4.59
C_{11} (GPa)	223[c]	238	246	256
C_{12} (GPa)	148[c]	166	137	177
C_{44} (GPa)	125[c]	130	123	148
γ (1 0 0) (mJ m^{-2})	1977[d]	2150		2139
γ (1 1 0) (mJ m^{-2})	2153[d]	2257		2256
γ (1 1 1) (mJ m^{-2})	1624[d]	1966		1579
V_{Ni} (eV/atom)	1.03[e]	1.57		0.79
V_{Al} (eV/atom)	1.995[e]	2.15		0.67

[a] [30],
[b] [31],
[c] [32],
[d] Model Electron Density Functional (MEDF) [33],
[d] [7],
[e] [34],
[f] [8].

Table 3. Properties of NiAl computed using EAM and COMB3 potentials compared to the results of experimental measurements.

	Expt.[a,b,c]	EAM Pun–Mishin[d]	COMB3 (this work)
a(Å)	2.88[a]	2.83	2.93
E_c (eV/atom)	−4.50[b]	−4.51	−4.44
C_{11} (GPa)	199[c]	191	154
C_{12} (GPa)	137[c]	143	114
C_{44} (GPa)	116[c]	121	134

[a] [21],
[b] [31],
[c] [35],
[d] [7].

with the fitting data set for the cohesive energy (E_c) and lattice constant (a_0) as indicated in table 4.

3. Results and discussion

3.1. Mechanical properties of Ni

The slip system in an FCC metal such as Ni is $\frac{a}{2}<\bar{1}\,1\,0>\{1\,1\,1\}$; the magnitude of the Burgers vector for these dislocations should be $a/\sqrt{2}$. However, it is well known that glide in FCC metals occurs by the movement of two partial dislocations [39], which are produced from the dissociation of the $\frac{a}{2}[\bar{1}\,1\,0]$ dislocations as indicated in equation (3).

$$\frac{a}{2}[\bar{1}\,1\,0] \rightarrow \frac{a}{6}[\bar{2}\,1\,1] + \frac{a}{6}[\bar{1}\,2\,\bar{1}] \quad (3)$$

The dislocations so produced are known as Shockley partials with a Burgers vector magnitude of $a/\sqrt{6}$, and the region between them is the stacking fault region. The stacking fault energy (SFE) is the energy per unit area of the planar defect between the two partials denoted by γ_{SF}. An accurate representation of the stacking fault energies is required for the potential to reproduce the correct deformation behaviour. The ability of COMB3 to capture this behaviour is illustrated in figure 1.

Table 4. Properties of NiO computed using the present COMB3 potential.

	Expt.[a,b]	DFT[c]	COMB3 (this work)
a (Å)	4.17[a]	4.19	4.15
E_c (eV/atom)	−4.75[b]	−5.8	−4.09

[a] [36],
[b] [37],
[c] [38].

3.2. Defect properties of Ni_3Al

3.2.1. Prediction of planar faults. The COMB3 potential developed in this work predicts properties of Ni_3Al that were not included in the fitting process reasonably well. These include the complex stacking fault (CSF) energy on the (1 1 1) plane and anti-phase boundary (APB) energies on the (1 1 1) and (1 0 0) plane. These are provided in table 5.

In general, the $<1\,1\,0>$ dislocations in Ni_3Al are called superdislocations as their Burgers vector is a [1 1 0] instead of $\frac{1}{2}$ a [1 1 0] as the latter type of slip would lead to an APB. This results in a superdislocation splitting into two superpartials that are bounded by an APB on the (1 1 1) plane. The larger slip vector accounts for the larger dislocation energy. This is the reason for the high strength of the Ni-base superalloys. The CSF has a Burgers vector of $\frac{1}{6}$ a $[\bar{2}\,1\,1]$, and it leads to the formation of an APB at the fault. This is analogous to the splitting of an FCC dislocation into Shockley partials as in equation (3).

The *yield stress anomaly* [2] is related to the APB(1 0 0) energy which has been shown to be lower than the APB(1 1 1) energy. At high temperatures, the dislocations may acquire sufficient energy to move from the glissile (1 1 1) to the sessile (1 0 0) planes. When that happens, an APB(1 0 0) forms instead of APB(1 1 1) which has a smaller energy as shown in table 5. This configuration, however gets locked to form the Kear–Wilsdorf locks [43, 44] leading to the enhanced

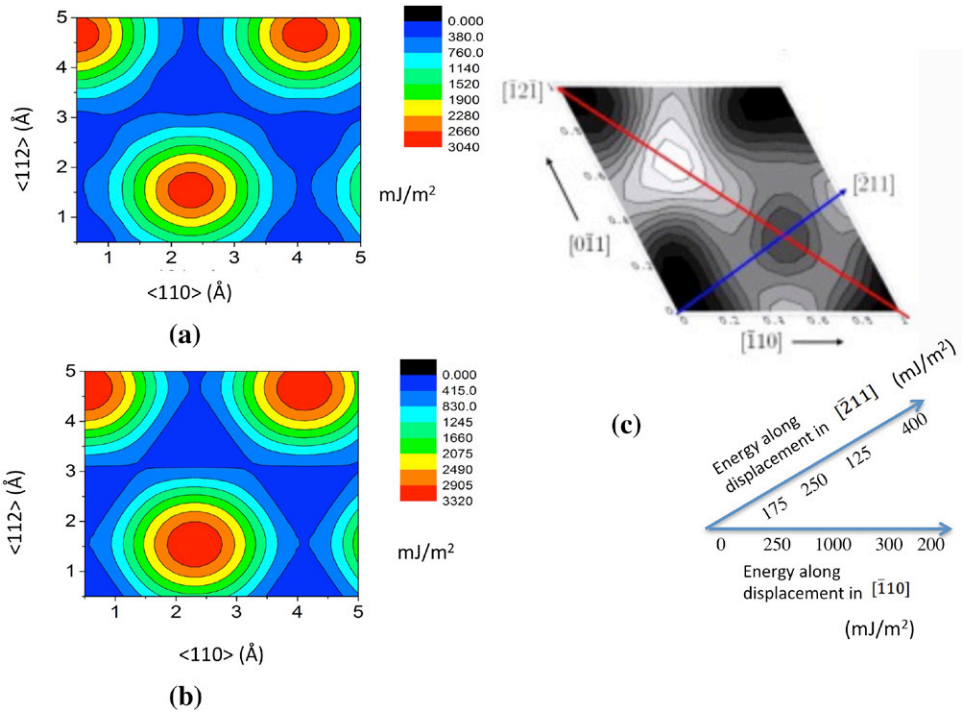

Figure 1. Contour plot showing the stacking fault barrier ($\gamma_{unstable}$) and the stacking fault energy (γ_{sf}) in the <1 1 0> and <1 1 2> directions as predicted by (a) COMB3 and (b) EAM Ni [27], and (c) DFT-GGA from [25] (figure used with permission).

Table 5. Planar faults in Ni_3Al and their energies (mJ m^{-2}) from experiments, DFT, EAM and COMB3.

	Expt.[a]	*Ab initio*[b,c]	EAM (Pun–Mishin)[d]	COMB3 (this work)
CSF (1 1 1)	235	225[b]	193	178
APB (1 1 1)	175	210[b]	249	311
APB (1 0 0)	104	121[c]	74	199

[a] [40],
[b] [41],
[c] [42],
[d] [7].

strength of the superalloys at higher temperatures. The present COMB3 potential is correctly able to reproduce this feature, which is critical to describing the high temperature behaviour of Ni_3Al.

3.2.2. Misfit dislocations at the γ–γ′ interface. The current potential was used to investigate the dislocation structure of Ni/Ni_3Al interface, which has been previously investigated using the Voter–Chen EAM potential by Xie *et al* [45] and Zhu *et al* [46] MD simulations were carried out at 300 K with an NVT ensemble indicated in the following setup (figure 2). After relaxation at 300 K, a shear stress was applied on the top and bottom rigid layers by giving a velocity of 0.005 Å ps^{-1} to the atoms in these layers. The simulation was carried out using the LAMMPS software [47].

Figure 3 illustrates the pattern of misfit dislocation indicated by crisscrossed lines that formed just after the relaxation. The dislocation lines form a kink at the point of intersections, as shown in figure 3(b). This is in agreement with the MD results from Zhu *et al* [46] using the Voter–Chen EAM potential for Ni_3Al [8].

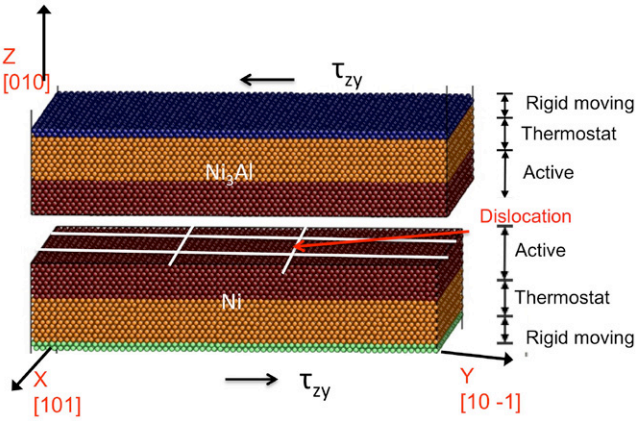

Figure 2. Simulation setup of a (1 1 0) interface of Ni and Ni_3Al with a total of 179 600 atoms after relaxation misfit dislocations, indicated by white lines are predicted to form. The figure illustrates the (i) rigid-moving layers where the shear stress was applied, (ii) thermostat region where temperature was fixed, and (iii) the active region where atoms are allowed to evolve without additional constraints.

Xie *et al* [45] suggested that the kinks nucleate at the intersection of the misfit dislocations due to a potential energy difference between the atoms at the core of dislocations and the atoms on the misfit dislocations. The results predicted here with the COMB3 potential are consistent with this finding as the atoms near the misfit dislocations have a larger potential energy than those away from the intersections. This is indicated schematically in figure 4.

These results indicate the present COMB3 potential is able to model the interfacial behaviour behaviour of the Ni (1 1 0)–Ni_3Al (1 1 0) as shown in some of the existing MD results.

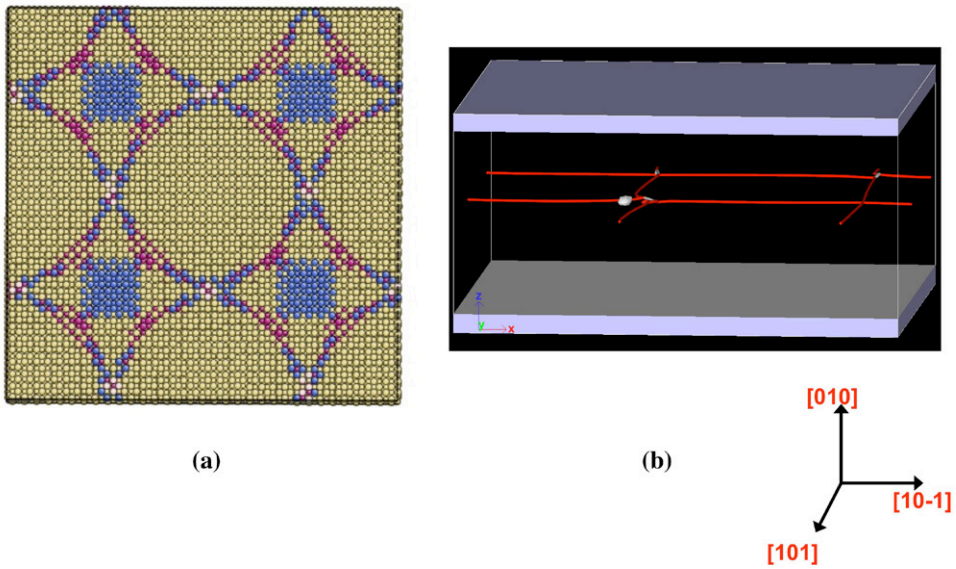

Figure 3. Structure of misfit dislocation that forms at the γ–γ interface. (a) Coordination colour-coded top view of the interface where yellow atoms are regular FCC atoms with coordination of 12, pink are atoms with coordination of 11, and blue atoms have a coordination of 13 (generated by atomeye [48]). (b) Only the dislocation lines and the kinks generated by the dislocation extraction algorithm [49] are illustrated for clarity.

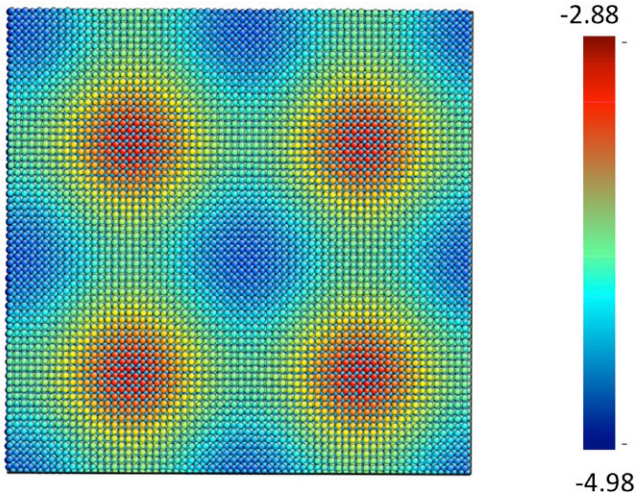

Figure 4. Potential energy/atom (in eV) colour-coded map of the interface illustrated in figure 3(a).

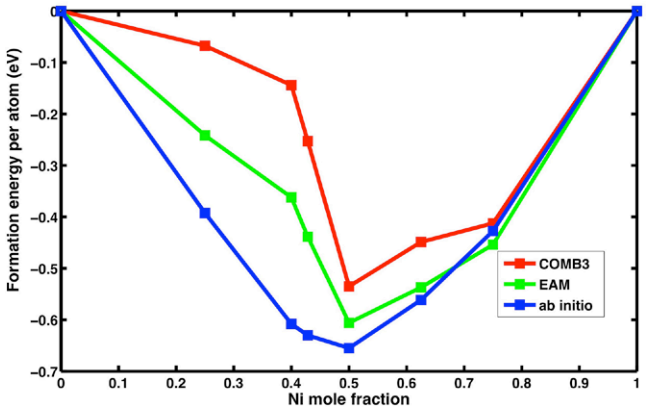

Figure 5. Formation energy/atom for different Ni–Al phases as calculated from COMB3, EAM Pun–Mishin [7] and DFT [51].

3.2.3. Charge distribution around vacancies. As discussed above, the COMB3 potential is able to dynamically predict changes to the atomic charges. Charges are not expected to play a significant role in determining the properties of a pure intermetallic compound. However, the presence of defects and impurities such as oxygen, might lead to small charge transfer. The calculations with COMB3 predict charges of −0.083e on Ni atoms and +0.25e on Al atoms in defect-free Ni_3Al. In general, the charges in COMB3 are lower than Bader charges [50] computed using DFT. In the vicinity of an Al vacancy, the charge distribution is more or less the same as the perfect Ni_3Al. Similar trends are predicted in DFT calculations, with little change in the Bader charges on the Ni atoms surrounding the Al vacancy and the Al atoms predicted to have nearly the same charge as in the defect-free system. Similarly, in the case of a Ni vacancy, both COMB3 and DFT predict very small changes to the charges on the Ni and Al atoms in the vicinity of the vacancy.

3.3. Ni–Al phase stability

The potential was tested across the Ni–Al phase diagram to predict the formation energies of different phases. In general, the formation energy can be defined as the enthalpy of the reaction as indicated in equation (4).

$$\Delta H_f = x\mathrm{Ni} + y\mathrm{Ni} \rightarrow \mathrm{Ni}_x\mathrm{Al}_y \tag{4}$$

Thus the heat of formation per atom would be $\Delta H_f/(x+y)$ for each Ni–Al phase. These formation energies are shown schematically in figure 5. It should be emphasized that no binary phase other than Ni_3Al and NiAl were included in the fitting database so the heats of formation for all other phases are pure predictions of the COMB3 potential. It can be seen clearly that the relative trend of the formation energy for all

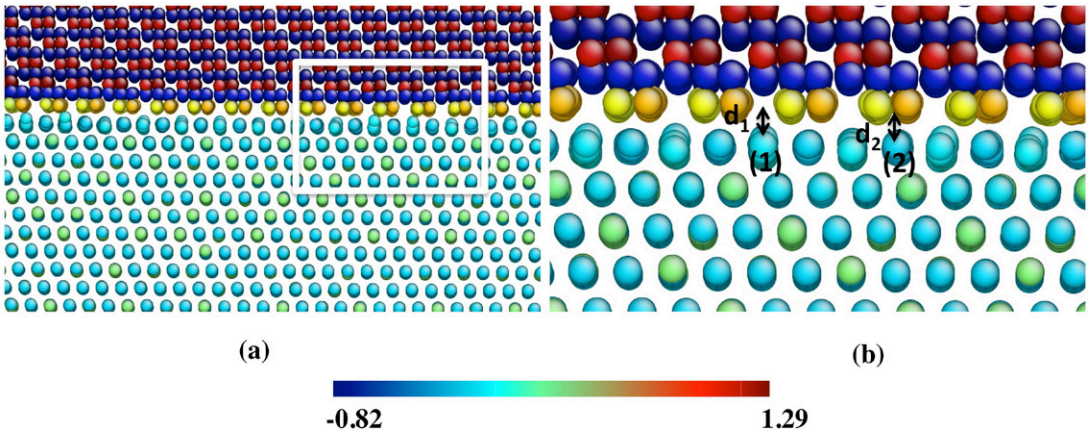

Figure 6. (a) $Ni_3Al(1\,1\,1)$–$Al_2O_3(0\,0\,0\,1)$ interface with the atoms colour-coded according to charge (elementary charge unit). (b) Close-up of the square from (a) to illustrate the variation of the interface distance at two different sites.

the phases are similar to the predictions of DFT and EAM potential by Pun and Mishin. However, it must be highlighted that unlike DFT, the EAM and COMB3 potentials do not predict the Al-rich Ni–Al phases to be the most stable for that composition. This may be attributed to the limitations associated with classical potentials in accurately describing the long-range Al–Al interactions necessary to correctly describe the Al-rich phases of the Ni–Al phase diagram. Given that the technologically important phases are Ni-rich, the level of agreement among the methods illustrated in figure 5 for Al-rich phases is acceptable.

3.4. Ni_3Al–Al_2O_3 interface

It is known that a protective coating of Al_2O_3 forms on the Ni-base superalloys at high temperatures [9]. This interface is thus critical to the performance of superalloys and addition of alloying elements in the alloy may modify this adhesion. The work of adhesion was calculated for three different strained interfaces of Ni_3Al $(1\,1\,1)$–Al_2O_3 $(0\,0\,0\,1)$ to better understand how strain influences bonding across the interface. The work of adhesion (W_{ad}) is defined as the energy released to create the interface as indicated in equation (5).

$$W_{ad} = \frac{E_{interface} - (E_{Ni_3Al} + E_{Al_2O_3})}{area_{interface}} \quad (5)$$

To build the interface, a system of 86 400 atoms of Ni_3Al and 52 920 atoms of Al_2O_3 was constructed with vacuum separating the two in the direction perpendicular to the interface. Each of the two surfaces and the interface were relaxed at 0.1 K using the NVT ensemble using the LAMMPS software [47]. The Nose-Hover thermostat was used with a temperature-damping constant of 0.01 ps. A close-up view of the relaxed Ni_3Al $(1\,1\,1)$–Al_2O_3 $(0\,0\,0\,1)$ interface is provided in figure 6(a).

Strain was applied to the Ni_3Al structure to match the interface dimensions. Accordingly, 20 units cells of Ni_3Al were used in each of the $[1\,1\,2]$ and $[1\,1\,0]$ directions for 21 × 21 unit cells of Al_2O_3. In the $[1\,1\,1]$ direction, there were 9 unit cells of Ni_3Al and 2 unit cells of Al_2O_3. The results are given in table 6. It can be seen that the cohesion is maximized around

Table 6. Calculated W_{ad} in COMB3 for different strained interfaces.

Case	Strain (%)	W_{ad} (J/m^2) COMB3 (this work)	W_{ad} (J m^{-2}) exp.[a]
A	0.22	1.81	1.76
B	0.50	1.85	
C	0.76	1.65	

[a] [53].

0.5% strain (Case B), which is consistent with experimental findings. This W_{ad} is greater than the unstrained W_{ad} for the Ni $(1\,1\,1)$–Al_2O_3 $(0\,0\,0\,1)$ interface, which is experimentally determined to be 1.1 J m^{-2} [52] and 1.17 J m^{-2} when calculated from contact angle measurements [53]. DFT predicts the W_{ad} for Ni $(1\,1\,1)$–Al_2O_3 $(0\,0\,0\,1)$ to be 1.30 J m^{-2} [54]. From all these results, we can conclude that the cohesion is greater at the Ni_3Al $(1\,1\,1)$–Al_2O_3 $(0\,0\,0\,1)$ interface than that at Ni $(1\,1\,1)$–Al_2O_3 $(0\,0\,0\,1)$.

3.4.1. Variation of charge across the interface. It is established that in Ni_3Al, Ni acquires a partial negative charge while Al acquires a partial positive charge [55]. Since the COMB3 potential includes dynamic charge-transfer, the charge landscape can be visualized across the Ni_3Al $(1\,1\,1)$–Al_2O_3 $(0\,0\,0\,1)$ interface as in figure 6(a). The charges on Al and O in the bulk Al_2O_3 layers are ~1.14e and ~ −0.7e, respectively. At the interface, Al atoms have a reduced positive charge of ~0.7e suggesting some charge transfer across the interface from Al in the Al_2O_3 to Ni in the Ni_3Al. This is found to be the case as Ni atoms at the interface have ~ −0.05e charge, while Al atoms have a small positive charge.

The COMB3 potential predicts the equilibrium distance between the Ni_3Al and Al_2O_3 to be 1.8 Å (d_1) at site (1) and 2.42 Å (d_2) at site (2) in figure 6(b). It can be concluded that the Ni atoms at site (1) from Ni_3Al want to get closer to the Al_2O_3 layer directly below the O atom, whereas Ni atoms at site (2) have another Al atom on top of them which limits the equilibrium distance to be around 2.42 Å. The (d_1) distance computed from DFT was predicted to be 1.86 Å for the Ni $(1\,1\,1)$–Al_2O_3 $(0\,0\,0\,1)$ interface by Zhang *et al* [54]

and stability was attributed to the polarization of Ni atoms by O atoms across the interface. The same argument could be applied to the Ni-rich intermetallic Ni_3Al (1 1 1)–Al_2O_3 (0 0 0 1) interface.

Thus, the suite of COMB3 potentials, including the newly parameterized potential for the Ni–Al system, can be used to model interfaces such as Ni_3Al–Al_2O_3. They can also predict resulting charge transfer between metals as the distance between them decreases due to the modified Charge Barrier function shown in equation (2).

4. Conclusions

We have presented an interatomic potential to simulate the binary Ni–Al system within the COMB3 formalism. The Ni–Al potential presented in this work is able to reproduce a range of physical properties of Ni_3Al and NiAl and the correct trend of formation energies of other Ni–Al phases as indicated on the phase diagram. The results are in good agreement with *ab initio* data and results from the EAM potential developed by Pun and Mishin [7]. Specifically for Ni_3Al, which is the primary phase of interest, we are able to show the reasonable surface and defect properties. Also, the potential is able to predict various planar defects that are essential for a correct behaviour of Ni_3Al in superalloys. Furthermore, we have parameterized the potential so that we can model Ni_3Al–Al_2O_3 interfaces. On a more important note, the ability to capture charge transfer makes the current COMB3 potential a unique choice for their system that can be used in combination with other COMB3 potentials to carry out a variety of classical MD simulations.

Acknowledgments

We gratefully acknowledge the support of the Air Force Office of Scientific Research through Grant # FA9550-12-1-0456. A K also acknowledges fruitful discussions with Prof Y Mishin of George Mason University.

References

[1] Betteridge W and Shaw S W K 1987 *Mater. Sci. Technol.* **3** 682–94
[2] Reed R C 2006 *The Superalloys Fundamentals and Applications* (Cambridge: Cambridge University Press)
[3] Darolia R 1991 *JOM* **43** 44–9
[4] Car R and Parrinello M 1985 *Phys. Rev. Lett.* **55** 2471–4
[5] Alder B J and Wainwright T E 1957 *J. Chem. Phys.* **27** 1208–9
[6] Alder B J and Wainwright T E 1959 *J. Chem. Phys* **31** 459–66
[7] Purja Pun G P and Mishin Y 2009 *Philos. Mag.* **89** 3245–67
[8] Voter A F and Chen S P 1986 *MRS Online Proc. Lib.* **82** 175–80
[9] Hayashi S and Gleeson B 2012 *Oxid. Met.* **77** 237–51
[10] Clarke D R, Oechsner M and Padture N P 2012 *Mater. Res. Bull.* **37** 891–8
[11] Phillpot S R and Sinnott S B 2009 *Science* **325** 1634–5
[12] Liang T, Shan T-R, Cheng Y-T, Devine B D, Noordhoek M, Li Y, Lu Z, Phillpot S R and Sinnott S B 2013 *Mater. Sci. Eng.* R **74** 255–79
[13] Choudhary K, Liang T, Chernatynskiy A, Lu Z, Goyal A, Phillpot S R and Sinnott S B 2015 *J. Phys.: Condens. Matter* **27** 015003
[14] Choudhary K, Liang T, Chernatynskiy A, Phillpot S R and Sinnott S B 2015 *J. Phys.: Condens. Matter* **27** 305004
[15] Devine B, Shan T-R, Cheng Y-T, McGaughey A J H, Lee M, Phillpot S R and Sinnott S B 2011 *Phys. Rev.* B **84** 125308
[16] Tersoff J 1988 *Phys. Rev.* B **37** 6991–7000
[17] Perdew J P, Burke K and Ernzerhof M 1996 *Phys. Rev. Lett.* **77** 3865–8
[18] Perdew J P, Burke K and Ernzerhof M 1997 *Phys. Rev. Lett.* **78** 1396
[19] Martinez J A, Yilmaz D E, Liang T, Sinnott S B and Phillpot S R 2013 *Curr. Opin. Solid State Mater. Sci.* **17** 263–70
[20] Nelder J A and Mead R 1965 *Comput. J.* **7** 308–13
[21] Kittel C 1986 *Introduction to Solid State Physics* 6th edn (New York: Wiley)
[22] Smith C J (ed) 1976 *Metal Reference Book* (London: Butterworth)
[23] Simmons G and Wang H 1971 *Single Crystal Elastic Constants and Calculated Aggregate Properties: A Handbook* (Cambridge, MA: MIT Press)
[24] Vitos L, Ruban A V, Skriver H L and Kollár J 1998 *Surf. Sci.* **411** 186–202
[25] Datta A, Waghmare U V and Ramamurty U 2009 *Scr. Mater.* **60** 124–27
[26] Wycisk W and Feller-Kniepmeier M 1978 *J. Nucl. Mater.* **69–70** 616–9
[27] Mishin Y, Farkas D, Mehl M J and Papaconstantopoulos D A 1999 *Phys. Rev.* B **59** 3393–407
[28] Lee B-J, Shim J-H and Baskes M I 2003 *Phys. Rev.* B **68** 144112
[29] Jonathan A Z, Huajian G and Farid F A 2000 *Modelling Simul. Mater. Sci. Eng.* **8** 103
[30] Raju S V, Oni A A, Godwal B K, Yan J, Drozd V, Srinivasan S, LeBeau J M, Rajan K and Saxena S K 2015 *J. Alloys Compd.* **619** 616–20
[31] Hultgren R, Desai P D, Hawkins D T, Gleiser M and Kelley K K 1973 *Selected Values of the Thermodynamic Properties of the Binary Alloys* (Metals Park, OH: ASM)
[32] Kayser F and Stassis C 1981 *Phys. Status Solidi* a **64** 335–42
[33] Kuznetsov V M, Kadyrov R I and Rudenskii G E 1998 *J. Mater. Sci. Technol.* **14** 320–22
[34] Ruban A V, Popov V A, Portnoi V K and Bogdanov V I 2013 *Philos. Mag.* **94** 20–34
[35] Rusović N and Warlimont H 1977 *Phys. Status Solidi a* **44** 609–19
[36] Wyckoff R W G 1964 *Crystal Structures* (New York: Interscience)
[37] Barin I 1989 *Thermochemical Data of Pure Substances* (Cambridge, MA: VCH)
[38] Dudarev S L, Botton G A, Savrasov S Y, Szotek Z, Temmerman W M and Sutton A P 1998 *Phys. Status Solidi* a **166** 429–43
[39] Hirth J P and Lothe J 1982 *Theory of Dislocations* 2nd edn (New York: Wiley)
[40] Karnthaler H P, Mühlbacher E T and Rentenberger C 1996 *Acta Mater.* **44** 547–60
[41] Mryasov O N, Gornostyrev Y N, van Schilfgaarde M and Freeman A J 2002 *Acta Mater.* **50** 4545–54
[42] Kohlhammer S, Fähnle M and Schoeck G 1998 *Scr. Mater.* **39** 359–63
[43] Caillard D and Couret A 1996 Ordered alloys *Dislocations in Solids* vol 10 ed F R N Nabarro and M S Duesbery (Amsterdam: Elsevier) pp 69–134

[44] Veyssière P and Saada G 1996 Ordered alloys *Dislocations in Solids* vol 10 ed F R N Nabarro and M S Duesbery (Amsterdam: Elsevier) pp 253–441
[45] Hong-Xian X, Chong-Yu W and Tao Y 2009 *Modelling Simul. Mater. Sci. Eng.* **17** 055007
[46] Zhu T and Wang C-Y 2005 *Phys. Rev.* B **72** 014111
[47] Plimpton S 1995 *J. Comput. Phys.* **117** 1–19
[48] Ju L 2003 *Modelling Simul. Mater. Sci. Eng.* **11** 173
[49] Stukowski A 2010 *Modelling Simul. Mater. Sci. Eng.* **18** 015012
[50] Tang W, Sanville E and Henkelman G 2009 *J. Phys.: Condens. Matter* **21** 084204
[51] Jain A, Hautier G, Ong S P, Moore C J, Fischer C C, Persson K A and Ceder G 2011 *Phys. Rev.* B **84** 045115
[52] Merlin V and Eustathopoulos N 1995 *J. Mater. Sci.* **30** 3619–24
[53] Saiz E, Cannon R M and Tomsia A P 1999 *Acta Mater.* **47** 4209–20
[54] Zhang W, Smith J R and Evans A G 2002 *Acta Mater.* **50** 3803–16
[55] Ravindran P, Subramoniam G and Asokamani R 1996 *Phys. Rev.* B **53** 1129–37